Quadratic nonlinear response to 1.56-μm continuous wave laser in semi-insulating GaAs

Xiuhuan Liu (刘秀环)[1*], Yi Li (李 一)[1], Zhanguo Chen (陈占国)[2], Mingli Li (李明利)[1], Gang Jia (贾 刚)[2], Yanjun Gao (高延军)[2], Lixin Hou (侯丽新)[2], Shuang Feng (冯 双)[2], Xinlu Li (李鑫璐)[2], and Qi Wang(王 琦)[2]

[1]*College of Communication Engineering, Jilin University, Changchun 130012, China*

[2]*State Key Laboratory on Integrated Optoelectronics, College of Electronic Science and Engineering, Jilin University, Changchun 130012, China*

[*]*Corresponding author: xhliu@jlu.edu.cn*

Received July 8, 2013; accepted September 23, 2013; posted online, October 23, 2013

The nonlinear photoresponse to a 1.56-μm infrared continuous wave laser in semi-insulating (SI) gallium-marsenide (GaAs) is examined. The double-frequency absorption (DFA) is responsible for the nonlinear photoresponse based on the quadratic dependence of the photocurrent separately on the coupled optical power and bias voltage. The electric field-induced DFA remarkably affects the native DFA in SI GaAs. The surface electric field or the surface band-bending of SI GaAs significantly affects the magnitude variation of the photocurrent and dark current.

OCIS codes: 250.4390, 250.0040, 190.4400, 190.4350.
doi: 10.3788/COL201311.112501.

Gallium arsenide (GaAs) has been extensively applied in III–V compound semiconductors because of its associated mature technologies. GaAs is preferable to silicon in microelectronics and optoelectronics to some extent. GaAs is a semiconductor material widely used for laser emitting diode due to its direct band gap[1−3]. Additionally, it has been applied in photodetector fabrication by virtue of its outstanding electrical properties[4,5] and negative-electron-affinity GaAs photocathodes have also been extensively investigated[6]. Moreover, some high speed and monolithic microwave-integrated circuits based on semi-insulating (SI) GaAs have important functions in radar, electronic countermeasures,computers, satellite communications, optical communications, etc.[7]. InGaAsN quantum well (QW) lasers on GaAs with superior characteristics for addressing 1300 to 1550-nm spectral regimes have been reported[8−13]. However, the intrinsic GaAs photodetectors based on single-photon absorption are commonly unsuitable to the aforementioned spectral region which covers the other two main optical communication wavelengths of 1.3 and 1.5 μm because the GaAs bandgap is 1.43 eV corresponding to the absorption limit of 867-nm wavelength. Erlig *et al.*[4] reported an LT-GaAs detector with 451-fs response at 1.55 μm, which was attributed to two-photon absorption (TPA). Han *et al.*[5] reported that the high performance at 1.55 μm of an LT-GaAs resonant-cavity-enhanced photodetector was dominantly based on below band-gap absorption resulting from the transition between the midgap defect state and the conduction band. GaAs belongs to the 43-m symmetry group. Thus, both double-frequency absorption (DFA) (involved in the second-order nonlinear optical effects) and TPA (characterized by the third-order nonlinear optics) can occur in GaAs crystals when they are irradiated by intense lasers with a wavelength ranging from 0.88 to 1.76 μm.Furthermore, electric fields have significant effects on the native double-frequency effects in some III–V compound semiconductors[14−17].

Compared with the InGaAsN/GaAs QW technology for addressing 1300 to 1550-nm spectral regimes, we developed an alternative approach, in which a relatively simple-structured SI-GaAs sample was used to investigate the nonlinear response to a 1.56-μm infrared laser.In this letter, the nonlinear photoresponse of the SI GaAs crystal is studied according to the photocurrent generated from the sample. The surface band-bending or the surface electric field (SEF) substantially affects the photoresponse.

The hemispherical sample with a bottom of (001) plane was made of chromium (Cr)-doped SI GaAs which was provided by the General Research Institute for Nonferrous Metals (Beijing, China). The experimental setup was similar to that described in Ref. [18]. Two types of aluminum electrode configurations were fabricated on the bottom of the sample. One electrode comprised a homocentric inner metal disk and an outer metal ring, and the other consisted of a stripe and an arrow with the tip arranged at the center of the sample bottom and pointing perpendicularly to the stripe. The 1.56-μm infrared continuous wave laser was adjusted to travel along the normal orientation of the sample hemisphere and focused at the center of the bottom, where the nonlinear response to the 1.56-μm wavelength evidently occurred and was thus enhanced on account of the hemispherical solid immersion lens[19]. The photocurrent quadratic dependent on the optical power for each electrode configuration is illustrated in Figs. 1 and 2, which indicate the DFA or the TPA responsible for the nonlinear photoresponse in the sample. In the experiments, the sample was biased at 80 V, and the central electrode (the electrode fixed at the center of the sample bottom, i.e, the inner disk electrode or the tip electrode) was positively and negatively charged for each electrode configuration. The photocurrent generated from the sample is noticeably larger in the

case under the central electrode negatively charged than that in the case under the central electrode positively charged. This difference is attributed to the different surface band-bending of the SI GaAs crystal for the cases of two opposite bias directions.

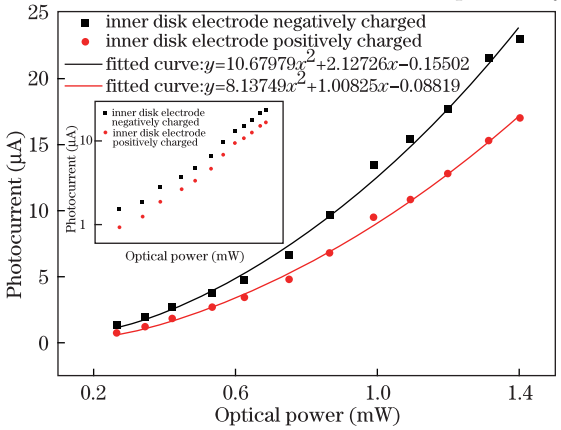

Fig. 1. Dependence of photocurrent on optical power for the electrode configuration of homocentric inner metal disk and outer metal ring. The inset shows the logarithmic relationship between the photocurrent and the incident power. The abscissas indicate the monitored power rather than the exact power coupled into the SI GaAs sample. The sample is biased at 80 V.

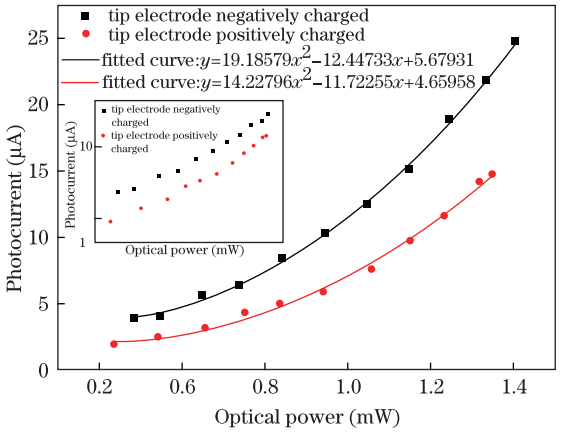

Fig. 2. Dependence of photocurrent on optical power for the stripe-arrow electrode configuration. The inset shows the logarithmic relationship between the photocurrent and the incident power. The abscissas indicate the monitored power rather than the exact power coupled into the SI GaAs sample. The sample is biased at 80 V.

Our SI GaAs sample was Cr-doped, but the electric or photoelectronic properties of Cr-doped SI GaAs are dominated not only by Cr but also by oxygen (O)[20−22]. The energy-level model and the surface band-bending of SI GaAs at room temperature deduced from Refs. [14, 20, 21, 23] are illustrated by Fig. 3(a). The E_c−0.84 eV and E_v+0.9 eV levels are associated with Cr, and the E_c−0.68 eV level is associated with O impurities[20,23]. In low-Cr SI GaAs, the deep O-donor level has a crucial effect on electric and optoelectronic properties, and the low-Cr SI GaAs is n type[21]. Fermi level E_f is located near E_c−0.65 eV[23], above the surface neutral level E_0, which is approximately one-third of the band gap above the valence band. The pinning of the Fermi level at the surface results in band-bending, and the SEF is along the crystalline [001] direction out of the SI GaAs bulk (Fig. 3(a)). The surface band-bending and the SEF are hardly affected by the physical metal–semiconductor contact because the surface state density is high enough for GaAs[24]. In our case, the nonlinear photoresponse substantially occurs in the region very close to the center of the (001) bottom of the SI GaAs sample. When the central electrode is negatively charged, the direction of the applied electric field around the center is approximately the same as that of the SEF inside the semiconductor, which consequently builds up the depletion electric field and enlarges the depletion region. The central electrode with a smaller area induces a steeper band-bending[25,26] near the center of the bottom when it is negatively charged, especially for the tip electrode with a sharp protrusion fixed at the center[27]. Consequently, the photo-generated carriers in the depletion region increases, and more electron–hole pairs are well separated and driven out of the sample under the stronger electric field. However, the variation of the photocurrent is contrary to the aforementioned analysis when the central electrode is positively charged. In the experiments, under the same bias and the same light exposure condition, the photocurrents are larger when the central electrode is negatively charged than those when the central electrode is positively charged (Figs. 1 and 2). The insets show the logarithmic relationship between the photocurrent and the incident optical power for each case.

The relationship between the photocurrent and the bias voltage was also investigated. The dependence of the photocurrent on the bias for the homocentric disk–ring electrode configuration is shown in Fig. 4, and a similar result for the stripe–arrow electrode configuration is illustrated in Fig. 5. The incident optical power was adjusted to be the same value for the two opposite bias directions in both cases. As shown in the two figures, the photocurrent rises slightly steeply as the bias voltage increases for the negatively charged central electrode, whereas it changes relatively slowly for the positively charged central electrode. This result agrees well with the theoretical analysis of the effect of SEF previously mentioned.

The insets in Figs. 4 and 5 show the variations in the dark currents versus bias voltages for the two electrode configurations, which are exactly opposite to those of the photocurrents. These experimental results can also be

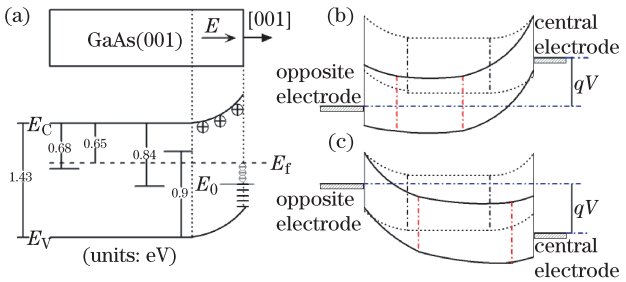

Fig. 3. Schematic diagrams of (a) energy-level model and surface band-bending for the SI GaAs at room temperature; (b) band-bending for the SI GaAs sample under the central eletrode negatively charged and (c) band-bending for the SI GaAs sample under the central electrode positively charged. In both (b) and (c), the solid line denotes the band-bending with the same voltage biased on the sample in two opposite

directions, respectively. The dotted line illustrates the surface band-bending without the applied voltages.

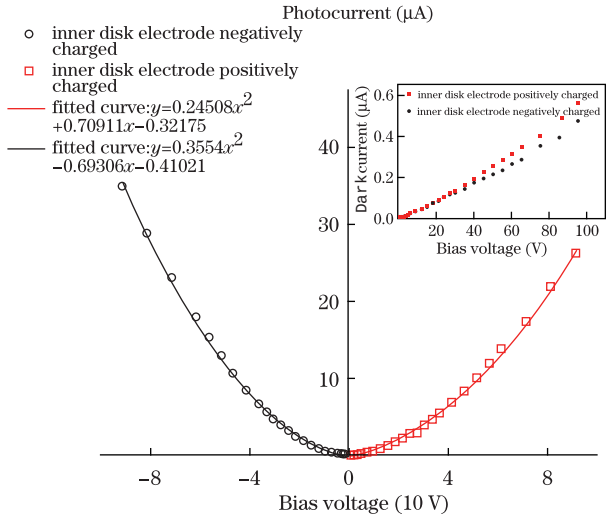

Fig. 4. Dependence of photocurrent on bias voltage for the electrode configuration of homocentric inner metal disk and outer metal ring. The inset shows the dark current versus bias voltage for the same electrode configuration.

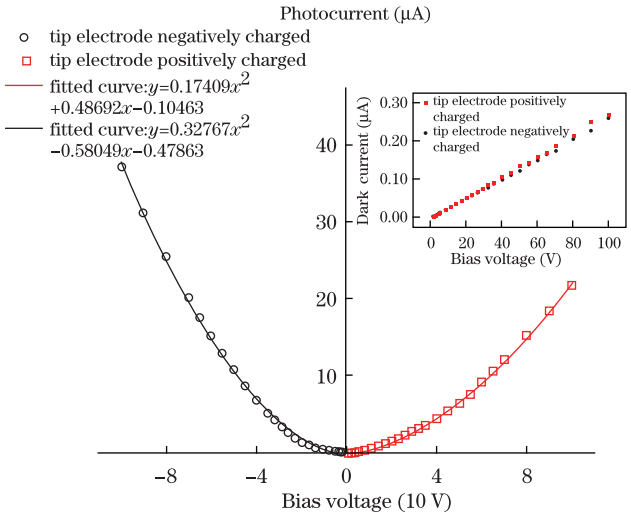

Fig. 5. Dependence of photocurrent on bias voltage for the stripe-arrow electrode configuration. The inset shows the dark current versus bias voltage for the same electrode configuration.

interpreted using the surface band-bending theory. For the negatively charged central electrode, the depletion region near the negative central electrode markedly expands because of the stronger applied electric field with an identical direction to the SEF induced by the smaller area of the central electrode. By contrast, the other depletion regien lightly decreases because of the weaker applied electric field with a direction opposite to that of the SEF induced by the larger area of the opposite electrode (Fig. 3(b)), which results in a larger effective series resistor for the sample. Then, a relatively small dark current is induced from the sample compared with the case under the central electrode positively charged at the same bias voltage, in which the depletion region near the center markedly decreases and the other slightly expands, as shown in Fig. 3(c). Thus, an induced smaller effective resistor for the sample induces a relatively large dark current. However, the difference in the magnitudes of the two dark currents at the same voltage in opposite bias directions is not very clear for the stripe–arrow electrode configuration, which may have originated from the comparable areas of the stripe and arrow electrodes (Fig. 5 inset). Biasing the central electrode negatively can lead to a larger ratio of photocurrent to dark current based on the variations in the magnitudes of the photocurrent and the dark current for both electrode configuration cases.

The profile of the photocurrent against bias voltage also satisfies second-order nonlinear fitting, as shown in Figs. 4 and 5. Combined with the results shown in Figs. 1 and 2, the quadratic dependence of the photocurrent on the bias voltage further clarifies that DFA is responsible for the photocurrent. This quadratic dependence is quite different from that of TPA in which the variation in the nonlinear photoresponse with applied bias exhibits saturation[18,28,29]. Moreover, the electric field-induced DFA evidently affects the native DFA in the SI GaAs sample. The intensity of electric-field-induced second-harmonic (EFISH) generation can be expressed as

$$I_{\rm v}(2w) \propto P_{\rm v}^2(2w) \propto |\chi^{(3)} E_{\rm v} E_w^2|^2, \tag{1}$$

where $I_{\rm v}(2w)$ represents the intensity of EFISH, $P_{\rm v}(2w)$ is the effective second-order polarization or the EFISH polarization, $\chi^{(3)}$ is the third-order susceptibility of the SI GaAs, E_w is the incident optical electric field, and $E_{\rm v}$ is the sum of the electric field induced by the applied voltage and the SEF. The total intensity of the second harmonic is consequently described as

$$\begin{aligned} I(2w) &\propto |\boldsymbol{P}_{\rm v}(2w) + \boldsymbol{P}_{\rm b}(2w)|^2 \\ &= P_{\rm v}^2(2w) + 2P_{\rm v}(2w)P_{\rm b}(2w)\cos\theta + P_b^2(2w), \end{aligned} \tag{2}$$

where $P_{\rm b}(2w)$ is the native second harmonic polarization or the background second harmonic polarization, and $P_{\rm b}(2w) \propto \chi^{(2)} E_w^2$. θ is the angle between the two polarization vectors, namely, $\boldsymbol{P}_{\rm v}(2w)$ and $\boldsymbol{P}_{\rm b}(2w)$, which are demonstrated to be parallel in our case. According to Eqs. (2) and (1), the total intensity of the second harmonic noticeably exhibits quadratic dependence on the applied electric field (accordingly on the bias voltage). The second harmonic corresponding to the fundamental wavelength 1.56 μm can be absorbed by the SI GaAs sample, and the number of the photo-generated carriers is proportional to the intensity of second harmonic $I(2w)$. Thus, the results shown in Figs. 4 and 5 perfectly demonstrate the quadratic dependence of the DFA on the bias voltage, which indicates that the electric field-induced DFA affects the native DFA in SI GaAs. Further investigation on this subject is still underway.

In conclusion, we investigate the nonlinear response to the 1.56-μm wavelength in SI GaAs. The DFA responsible for the photoresponse was determined based on the quadratic dependence of the photocurrent separately on the incident optical power and bias voltage. The electric field-induced DFA and the native DFA have important functions in the photoresponse in SI GaAs. The photocurrent improves relatively steeply as the bias voltage

increased for the negatively charged electrode compared with the positively charged electrode. The variation in the magnitude of the dark current is contrary to that of the photocurrent. These experimental phenomena are well interpreted by the contribution of the surface band-bending. The investigation of nonlinear response to communication wavelengths for SI GaAs material can facilitate photodetector fabrication, which will find potential applications in optical communications, Terahertz science, and autocorrelation measurements.

This work was supported by the Natural Science Foundation of Jilin Province (Nos. 201215019 and 201115026), the Collaborative Project of NSFC-RFBR (No. 61111120097), and the National Natural Science Foundation of China (Nos. 60976037 and 61077026).

References

1. K. Fujita, H. Ohnishi, P. O. Vaccaro, and T. Watanabe, Microelectronics J. **28,** 1019 (1997).
2. H. K. Choi, G. W. Turner, T. H. Windhorn, and B. Y. Tsaur, IEEE Electron. Device Lett. **EDL-7,** 500 (1986).
3. H. K. Choi, J. P. Mattia, G. W. Turner, and B. Y. Tsaur, IEEE Electron. Device Lett. **9,** 512 (1988).
4. H. Erlig, S. Wang, T. Azfar, A. Udupa, H. R. Fetterman, and D. C. Streit, Electron. Lett. **35,** 173 (1999).
5. Q. Han, Z. Niu, L. Peng, H. Ni, X. Yang, Y. Du, H. Zhao, R. Wu, and Q. Wang, Appl. Phys. Lett. **89,** 131104 (2006).
6. S. Zhang, L. Chen, and S. Zhuang, Chin. Opt. Lett. **10,** 110401 (2012).
7. J. Wang, S. Niu, T. Lan, C. Zhou, and Q. Sun, Science and Technology Innovation Herald **32,** 75 (2010) .
8. I. Vurgaftman, J. R. Meyer, N. Tansu, and L. J. Mawst, Appl. Phys. Lett. **83,** 2742 (2003).
9. N. Tansu, J. Yeh, and L. J. Mawst, IEEE J. Select. Topic. Quantum Electron. **9**, 1220 (2003).
10. N. Tansu, A. Quandt, M. Kanskar, W. Mulhearn, and L. J. Mawst, Appl. Phys. Lett. **83**, 18 (2003).
11. N. Tansu and L. J. Mawst, J. Appl. Phys. **97,** 054502 (2005).
12. J. W. Ferguson, P. Blood, P. M. Smowton, H. Bae, T. Sarmiento, J. S. Harris, N. Tansu, and L. J. Mawst, IEEE J. Quantum Electron. **47,** 870 (2011).
13. L. Xu, D. Patel, C. S. Menoni, J. Y. Yeh, L. J. Mawst, and N. Tansu, IEEE Photon. J. **4,** 2262 (2012).
14. J. Qi, M. S. Yeganeh, I. Koltover, A. G. Yodh, and W. M. Theis, Phys. Rev. Lett. **71,** 633 (1993).
15. T. A. Germer, K. W. Kolasiński, J. C. Stephenson, and L. J. Richer, Phys. Rev. B **55,** 10694 (1997).
16. K. A. Peterson and D. J. Kane, Opt. Lett. **26,** 438 (2001).
17. D. J. Kane and W. Wood, IEEE Photon. Technol. Lett. **18,** 1669 (2006).
18. X. Liu, Z. Chen, G. Jia, H. Wang, Y. Gao, and Y. Li, Chin. Phys. Lett. **28,** 114202 (2011).
19. D. A. Fletcher, K. B. Crozier, C. F. Quate, G. S. Kino, and K. E. Goodson, Appl. Phys. Lett. **77,** 2109 (2000).
20. A. L. Lin and R. H. Bube, J. Appl. Phys. **47,** 1859 (1976).
21. R. Zucca, J. Appl. Phys. **48,** 1987 (1977).
22. P. F. Lindquist, J. Appl. Phys. **48,** 1262 (1977).
23. K. Kitahara, N. Nakai, A. Shibatomi, and S. Ohkawa, Appl. Phys. Lett. **32**, 259 (1978).
24. E. Liu, B. Zhu, and J. Luo, *Semiconductor Physics* (Beijing Publishing House of Electronics Industry, Beijing, 2003).
25. A. Behnam, J. Johnson, Y. Choi, L. Noriega, M. G. Ertosun, Z. Wu, A. G. Rinzler, P. Kapur, K. C. Saraswat, and A. Ural, J. Appl. Phys. **103,** 114315 (2008).
26. J. H. Park and H. Yu, Opt. Lett. **36,** 1182 (2011).
27. M. Hamada, T. Teraji, and T. Ito, J. Appl. Phys. **107,** 063708 (2010).
28. T. K. Liang, H. K. Tsang, I. E. Day, J. Drake, A. P. Knights, and M. Asghari, Appl. Phys. Lett. **81,** 1323 (2002).
29. B. Shi, X. Liu, Z. Chen, G. Jia, K. Cao, Y. Zhang, S. Wang, C. Ren, and J. Zhao, Appl. Phys. B **93,** 873 (2008).